

A Low-Power 20-Gb/s Discrete-Time Analog Front-End for ADC-Based Serial Link Equalizers

Mostafa M. Ayesh¹, Sameh Ibrahim¹ and Mohamed M. Aboudina²
¹ EECE, Ain Shams University ² EECE, Cairo University

Abstract—This paper presents a discrete-time analog front-end for an analog-to-digital (ADC) based equalizers. The front-end uses a discrete-time linear equalizer (DTLE) and ultra-low-power 4-bit time-interleaved charge-steering flash ADC. The DTLE serves two functions; linear equalization and sampling and holding for the following charge-steering ADC. The ADC uses fully differential low-power clocked comparators. Low power in the comparators is achieved by embedding a dynamic latch into the core of a charge-steering pre-amplifier. The 20-Gb/s front-end is designed and simulated in a 65-nm CMOS technology. The flash ADC uses 4-stage interleaving and thus requires 4 DTLEs running at 5 Gb/s. A 5-Gb/s DTLE consumes 0.57 mW from a 1.2-V supply and the ADC consumes 15.5 mW from a 1-V supply at 20 GS/s for a total power dissipation of 17.78 mW or 0.89 pJ/bit. The ADC has an SNDR of 23.9 dB, an SFDR of 33.6 dB, and an effective number of bits (ENOB) of 3.67 bits for a sinusoidal input of frequency 9.84 GHz and amplitude 600 mV_{diff}.

Keywords—Charge-Steering, Preamplifier, Regeneration, Ultra-low power, Comparator, Flash ADC, High-speed ADC, Time-interleaved, ADC-based systems, Dynamic latch, Discrete-Time, Linear Equalizer.

I. INTRODUCTION

High-speed comparators with low-power consumption and small sensitivity are essential blocks in many applications that require very high sampling rates and low resolution such as data-storage read channels and wired communication systems [1]. As the demand for high rates increases, comparators must cope with this need while achieving as low power consumption and small area as possible. For example, recent communication links try to use ADC-based receivers which mainly depend on analog-to-digital converters (ADCs). However, power consumption remains a concern. A comparator is the main building block in any ADC. Improving its performance by reducing its kick-back noise and power consumption while maintaining high sampling rate will directly improve the whole ADC. As a result, the multi-standard reconfigurable systems which heavily depend on an ADC near the front end and digital blocks at the back end are becoming more common.

Time-interleaving has been widely used to allow for higher speed ADCs while keeping power consumption at reasonable levels. The power consumption overhead of interleaving becomes insignificant above certain frequencies when compared to the increase of the power consumption of a single-channel ADC.

The goal of the paper is to propose and analyze a novel topology, based on the charge-steering concept, for an ultra-low-power ultra-high-speed comparator. Then this comparator is used to build a low-power flash ADC to be used in a high-speed serial link ADC-based equalizer. A 4-bit 20-GS/s 4x time-interleaved flash ADC is used. Usually, serial link equalizers need some linear equalization to compensate for precursor inter-symbol interference (ISI), as a result, the design of the analog front-end of the equalizer is completed by adding discrete-time linear equalizer (DTLE) at the input.

The design of the DTLE is explained in section II. Section III discusses the charge-steering concept. The proposed fully differential comparator is discussed in section IV along with its proposed single-ended version and its delay analysis. Section V shows the designed charge-steering Flash ADC based on that comparator. The simulation results of the comparator, the ADC, and its front-end are given in section VI. Finally, the work is concluded in section VII.

II. DISCRETE-TIME LINEAR EQUALIZER

Since the analog input is changing at very high speeds, Flash ADC-comparators might samples the input at different instances due to the different types of mismatches. To overcome this issue, a sample-and-hold (S/H) circuit is needed at the input of the ADC to make sure that the introduced input to all of the comparators is the same. During the reset mode of the comparators, the sample-and-hold circuit samples the input then hold it for the comparators during the amplification and the regeneration modes [2].

For pre-cursor ISI equalization, many designs adopted the conventional continuous-time linear equalizer (CTLE) [3]. The main disadvantage of the CTLE is the direct and continuous path from supply to ground. That is why it is not a proper option for the low-power applications. A DTLE is a linear equalizer that replaces the conventional CTLE and its continuous-time nature to a discrete-time nature [2 - 3]. It could be seen as a combined continuous-time linear equalizer and a sample-and-hold circuit.

The resistive loads in a conventional CTLE are replaced with switched resistors and the conventional current sources are replaced with clocked current sources as shown in Figure 1. The circuit has two main modes of operation, the hold mode, and the track-and-equalize mode. When CLK signal is “High”, the track-and-equalize mode is activated. The clocked current

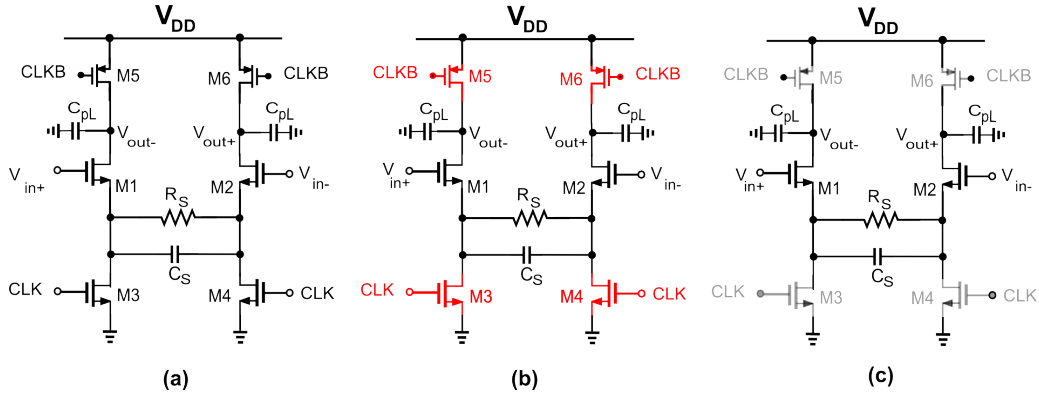


Fig. 1. (a) A Schematic of the DTLE Circuit. (b) The Track-and-Equalize Mode (CLK = “High”). (c) The Hold Mode (CLK = “Low”).

sources and the loading resistors are “ON”, hence the DTLE works as a peaking amplifier as shown in Figure 1 (b). When CLK signal goes “Low”, the circuit enters the hold mode. The clocked current sources are “OFF” and the switched resistors are at high impedance and hence the output values are almost not changing during this phase as presented in Figure 1 (c). This is good for the ADC to follow and cancels the need for a sample-and-hold circuit. As a result, power is saved.

However, the input devices are not instantly switched off because some time is needed to charge the tails nodes to switch off the input devices, so the output nodes face some leakage and the amplitude drops a little. Some reset NMOS transistors $M7$ and $M8$ might be added to rapidly charge the tail nodes and thus switch off the input devices during the hold mode. This will decrease the leakage of the output node and solve the issue as shown in Figure 2. The input at the end of the clock is sampled, processed and held.

The circuit is degenerated with a capacitor C_s which is the main reason for the gain peaking. This capacitor with the degeneration resistor R_s form a zero at ω_z and a pole ω_{p1} , and these are added to the existing pole at the output node at ω_{p2} . The locations of the poles and the zero are as following:

$$\omega_z = \frac{1}{R_s C_s} \quad (1)$$

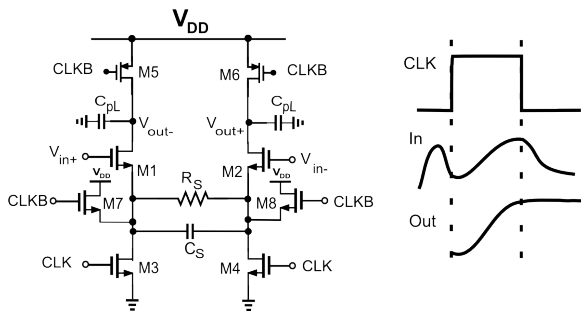


Fig. 2. The DTLE with Leakage Blockers.

$$\omega_{p1} = \frac{1 + (g_m + g_{mb})R_s/2}{R_s C_s} \quad (2)$$

$$\omega_{p2} = \frac{1}{R_d C_{pL}} \quad (3)$$

where R_d is the resistance of the clocked PMOS switch in the load that is kept in the linear region of operation.

$$R_d = \frac{1}{\mu_p C_{ox}(W/L)(|V_{GS}| - |V_{th}|)} \quad (4)$$

Some of the most important and meaningful quantities for the peaking amplifier is the DC gain, AC gain and the peaking it achieves. Peaking is defined as the ratio of the high-frequency gain to the low-frequency gain.

$$Gain_{DC} = \frac{(g_m + g_{mb})R_d}{1 + (g_m + g_{mb})R_s/2} \quad (5)$$

$$Gain_{Hi-freq} = g_m R_d \quad (6)$$

III. CHARGE-STEERING CONCEPT

Instead of using current-steering power-hungry circuits, discrete-time charge-steering circuits consume less power than their continuous-time current-steering counterparts, especially at high speeds. This advantage can be utilized in designing semi-analog circuits such as latches, demultiplexers, clock-and-data recovery (CDR) circuits, and comparators as well as mixed-mode systems such as ADCs [4]. The main concept is converting the continuous-time current-steering circuit to a discrete-time charge-steering topology as in [4]. The tail current source, as in Figure 3 (a), is replaced with a charge source, and the load resistors with switched capacitors. Discrete-time operation requires two switches in the tail path and two at the output nodes as shown in Figure 3 (b).

The operation of this charge-steering-based differential amplifier is divided into two phases; reset phase and amplification phase. In the reset phase, the tail capacitor is discharged while the output nodes are pre-charged to V_{DD} . In the amplification phase, the tail capacitor is connected to the tail node, drawing a current from the input pair while the outputs are disconnected from V_{DD} . Then, the input pair draws a differential current from the load capacitors in proportion to the differential input voltage. This results in an output voltage proportional to the input voltage. Figure 4 was introduced in [5] as a dynamic latch for digital signals utilizing charge-steering circuits. The extra back-to-back PMOS pair $M7$ - $M8$ helps in extending the swing of the original amplifier. This circuit cannot be used as a comparator for analog signals. The reason is that for small input signals, the input pair $M1$ - $M2$ is fighting against the regenerative latch $M7$ - $M8$ and will need a long time constant to produce an output. Hence, at high clock frequencies, the sensitivity of this circuit is compromised.

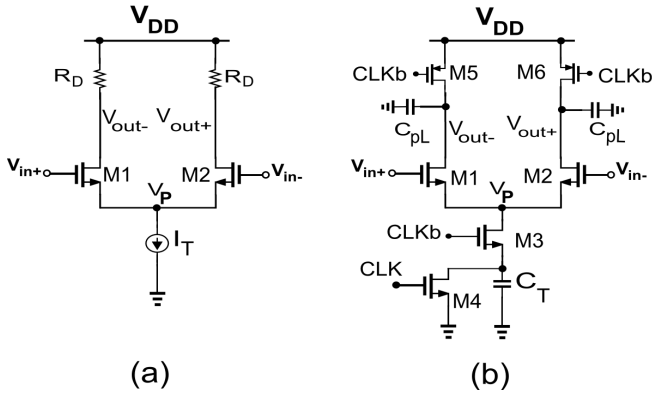


Fig. 3. Differential Pair Using: (a) Current-Steering. (b) Charge-Steering. [4]

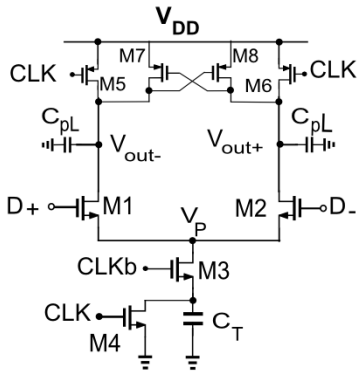


Fig. 4. A Schematic Diagram for a Charge-Steering Latch. [5]

IV. THE PROPOSED FULLY-DIFFERENTIAL COMPARATOR

The proposed comparator is utilizing the charge-steering concept as shown in Figure 5. The basic charge-steering amplifier consists of transistors $M1$ - $M6$, $M9$ - $M12$ and two tail capacitors C_T amplifies the input signal. In order to

regenerate the output signal, a regenerative latch might be added after this stage which will cause an increase in the power consumption of the comparator drastically. In this proposed design, an idea of an embedded regenerative latch as in [6] is used but it is turned “OFF” in the reset and amplification phases and is turned “ON” in the regeneration phase. This is achieved by switching the transistor $M13$ in Figure 5. $M13$ isolates the regenerative latch from both reset and amplification phases in order to avoid fighting. This results in an ultra-fast amplification for very low power consumption. The role of the embedded regenerative latch is to redistribute the differential charge increasing the output voltage. A new clocking scheme is introduced to facilitate the proposed operation. Figure 6 shows the proposed clocking scheme. The operation is divided into three phases of operation: reset phase, amplification phase, and regeneration phase. Figure 7 shows the proposed circuit in its three phases of operation.

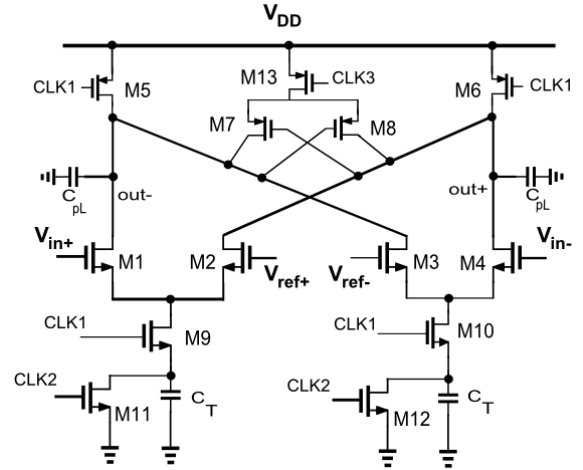


Fig. 5. Proposed Fully-Differential Latched Dynamic Charge-Steering Pre-Amplifier. [7]

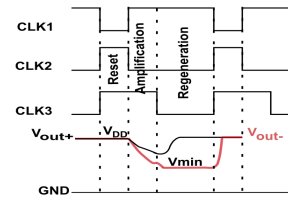


Fig. 6. Clocking Scheme for Different Phases. [7]

A. Reset phase

This is the initial phase shown in Figure 7 (a). It initializes the circuit when $CLK1$ is low, $CLK2$ is high and $CLK3$ is high leading to $M5$ and $M6$ being “ON” and pre-charging the two output nodes to V_{DD} such that $V_{out+} = V_{out-} = V_{DD}$. At the same time, $M9$ and $M10$ are “OFF” and the tail capacitors C_T are discharged to GND through $M11$ and $M12$ resulting in $V_{C_T} = 0$, where V_{C_T} is the voltage across the tail capacitor.

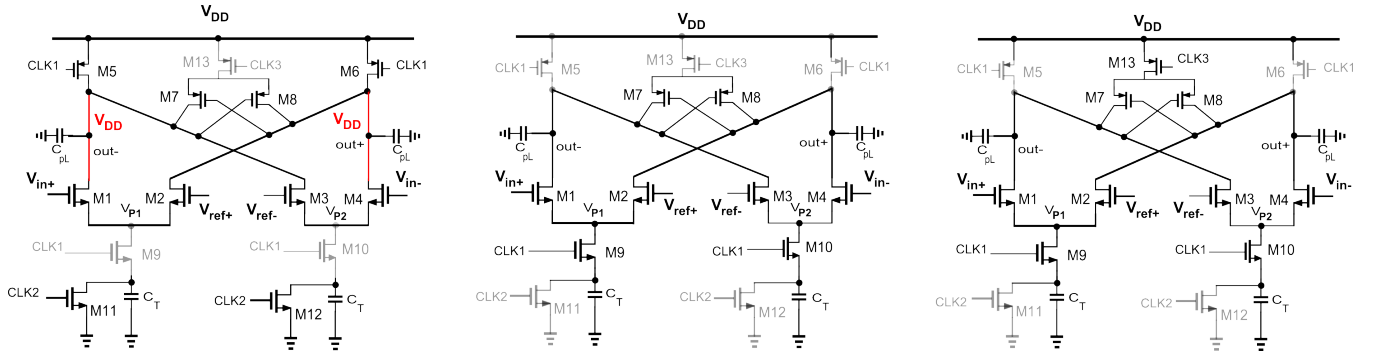


Fig. 7. The Proposed Comparator (a) Reset Phase. (b) Amplification Phase. (c) Regeneration Phase.

B. Amplification phase

In the second phase, CLK1 turns high and CLK2 turns low while CLK3 is still high leaving all nodes at a high impedance state as shown in Figure 7 (b). In this phase, the circuit acts like a differential amplifier typically as stated in section III. The steady state of the differential output is proportional to the input voltage. The gain is mainly governed by C_T and C_{pL} . Since there is no DC path to GND in this phase, the voltage difference is created by charge redistribution between the two output capacitors C_{pL} and the tail capacitors C_T while consuming little extra power consumption. At the end of this phase, the two output voltages are sitting at levels slightly higher than the voltage level V_{min} as shown in Figure 6. The output voltage difference is an amplified version of the input as explained before. The small-signal output voltage at the end of the amplification phase can be given by:

$$V_{out} = g_{m,avg} R_{out} V_{in} \quad (7)$$

Where $g_{m,avg}$ is the average transconductance of the input pair and R_{out} is the effective resistance of the switched capacitor structure resulting from charging and discharging of the load capacitors C_{pL} : $R_{out} = \frac{\Delta T}{C_{pL}}$. Where ΔT is the discharging time of C_{pL} which equals the charging time of the tail capacitor C_T to make V_p rises from zero to $V_{CM} - V_{TH} - \Delta V$ where ΔV is somewhat small and arbitrary voltage. ΔT is given in [9] as

$$\Delta T = \frac{C_T}{K} \frac{V_{CM} - V_{TH} - \Delta V}{(V_{CM} - V_{TH}) \Delta V} \quad (8)$$

where K is a physical constant of transistor parameters.

The output voltage at the end of the amplification phase can be given by:

$$V_{out} = 2 \times \frac{V_{CM} - V_{TH} - \Delta V}{V_{CM} - V_{TH} + \Delta V} \times \frac{C_T}{C_{pL}} \times V_{in} \quad (9)$$

C. Regeneration phase

The third phase shown in Figure 7 (c) starts when CLK3 turns low. M13 turns ON, thus M7 and M8 form a cross-coupled regenerative latch with an initial condition given by the final value of the amplification phase. The differential

output, hence, starts to grow exponential till it reaches its saturation limit where the upper limit is V_{DD} and the lower limit is V_{min} . The cross-coupled devices work on regenerating the output voltage by charge redistribution between C_T , C_{pL1} and C_{pL2} . Once one of the two outputs reaches V_{DD} (V_{out+}), the regeneration operation stops and M7 turns "OFF" keeping (V_{out-}) sitting at a voltage V_{min} . The cross-coupled pair will prevent the lower output to be pulled high and hence preserves the regenerated output till the next reset phase.

On one hand, higher C_T would lead to lower voltage levels after the charge-sharing operation taking place in the amplification phase. On the other hand, power consumption increases linearly with the C_T value. In this design, a capacitance value of 30 fF is chosen which resulted in an effective voltage gain at the end of amplification phase of 2.5 and a value of V_{min} equal to 40% of the supply. This proposed architecture combines the pre-amplification and the regeneration functions of a typical comparator circuit into one stage. It also relies on the concept of charge redistribution and re-using the stored charges to obtain the required output voltage at the end of each phase. The comparator is sensitive to very small input voltages at extremely high speeds by enabling the regeneration after the amplification phase is done. The circuit consumes very low power consumption since there is no direct path from V_{DD} to GND after the initial reset phase.

A single-ended version of the proposed comparator is shown in Figure 8. This single-ended circuit works the same as the differential circuit with same timing scheme. A single-ended version can be used with a single-ended input where a clocked comparator is needed and will be used for comparison with the conventional strongARM comparator.

D. Delay Analysis for the Proposed Circuit

According to the work published in [8], the total delay for the conventional StrongARM comparator is comprised of two time delays, t_0 and t_{latch} . In our proposed circuit. The delay t_0 represents the time taken in amplification phase which is the quarter of the clock cycle T_s . The delay t_{latch} is the time taken by cross-coupled latch to regenerate outputs to distinct values. It is defined as the time taken to have a voltage difference at

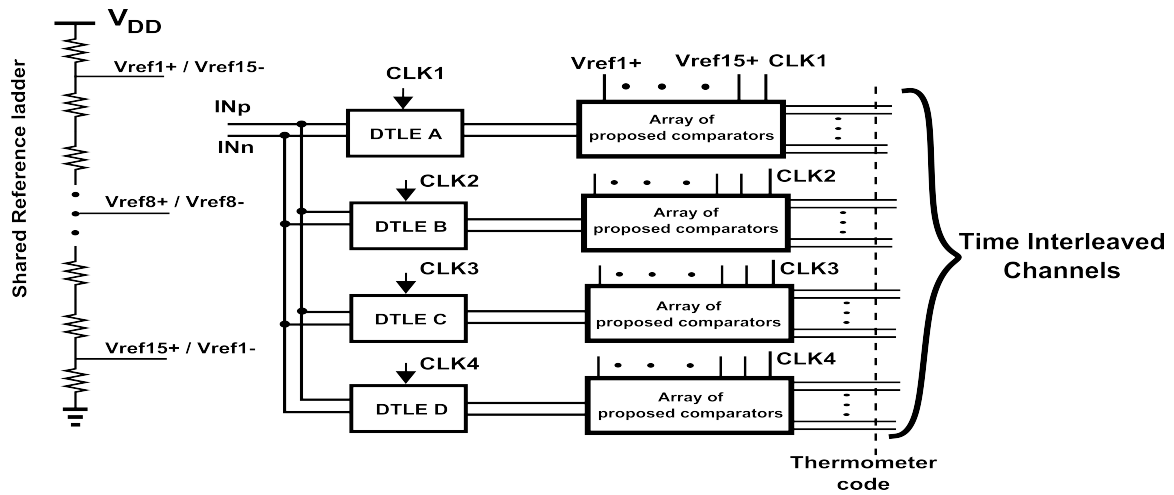


Fig. 9. Time-Interleaved ADC Architecture.

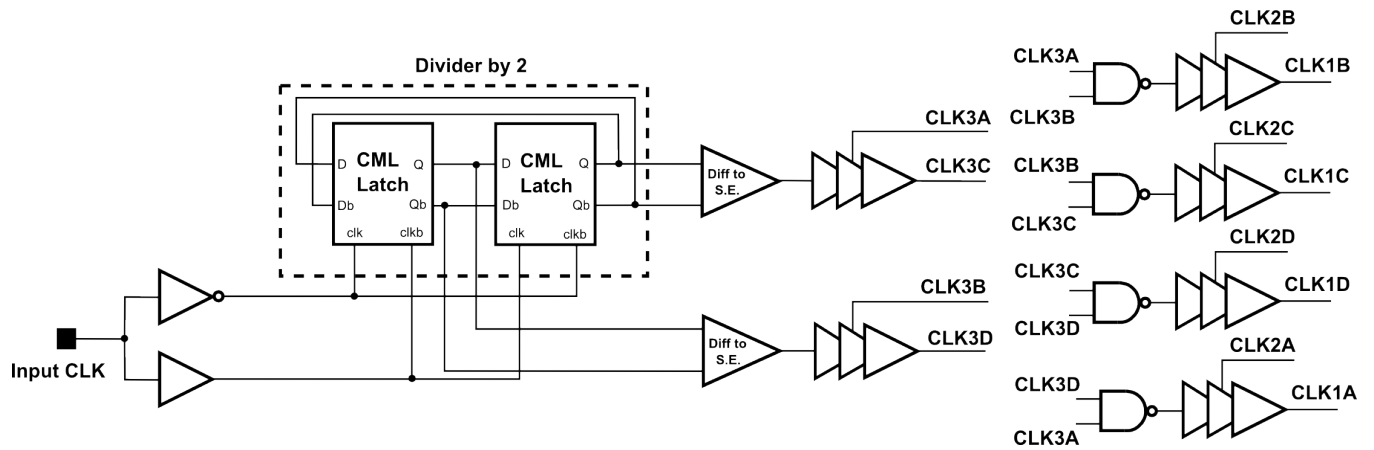


Fig. 10. The Designed Clocking System to Generate the Required Clocks.

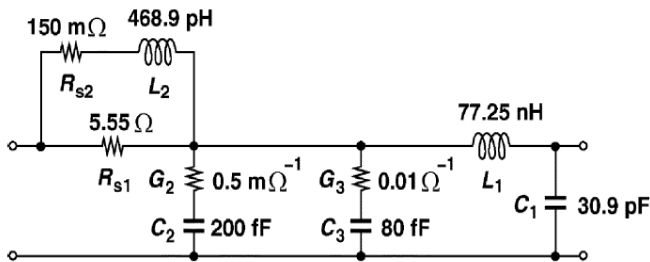


Fig. 11. A Schematic for Equivalent Model of 1-inch FR4 Channel. [3]

was transmitted through the channel with a 20-Gb/s rate and DTLE was running on 5-GHz clocks while consuming only 0.57 mW from a 1.2-V supply. The eye diagram at the end of the channel, i.e. input of the receiver, and the eye diagram after the DTLE are shown in Figure 12. The first eye diagram is totally closed, while the latter eye diagram has a vertical eye opening of 120 mV. Since the ADC has a differential dynamic

range of 600 mV_{pp} and a common-mode input voltage of 750 mV, the DTLE needs to be followed by a programmable gain amplifier (PGA) to match the DTLE output with the dynamic range and the input common-mode voltage of the ADC. In summary, Table I compares the designed DTLE with the prior work in the literature.

The proposed 5-GHz comparator shown in Figure 5 has been designed using a digital 65-nm CMOS technology. The total power consumption of the proposed fully differential comparator is 189 μ W and its single-ended version only consumes 66 μ W. Simulated waveforms of clocks and outputs are shown in Figure 13. The power consumption of the single-ended topology is split into 54 μ W for the reset and amplification phases and 12 μ W for the regeneration phase, whereas the differential comparator consumes 163 μ W and 26 μ W, respectively. In this comparator, Kick-back noise level is as tiny as 1 mV because outputs of the comparator core don't have rail to rail values.

TABLE I. DTLE PERFORMANCE COMPARISON.

Specification	[3]	[10]	[11]	This Work
Technology	130nm	32nm	90nm	65nm
Power Supply (V)	1.6	1.1	1.25	1.2
EQ. Architecture	Inductive-Loaded CTLE	CTLE + -ve C Bandwidth Extension	CTLE	Quarter-Rate DTLE
Data Rate (Gb/s)	10	12.5	8	5 (per channel)
Channel Loss (dB)	18	32	N/A	12
Gain @ Nyquist (dB)	N/A	10 (Input Stage + 2-CTLE Stages)	N/A	20
Power (mW)	41	5.25	2.32	0.57*

*for a single DTLE

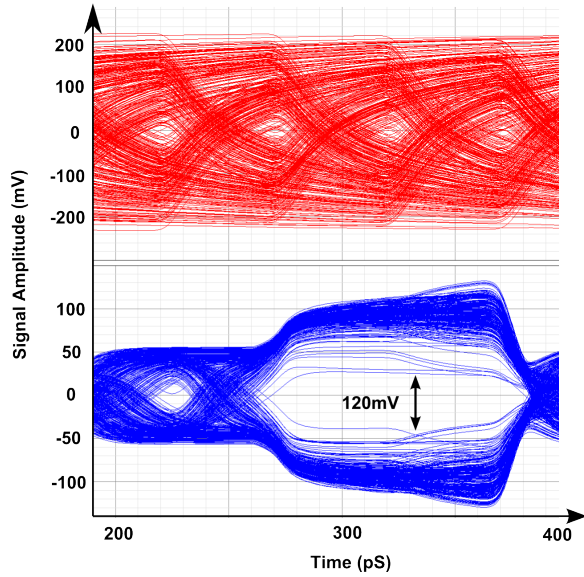


Fig. 12. The Eye Diagrams at the Receiver Input (Upper) and After DTLE.

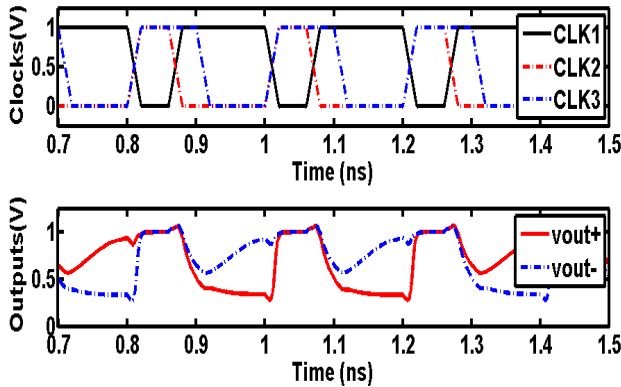


Fig. 13. Simulation Results for Comparator Outputs Vs. Clocking Scheme.

Monte-Carlo simulation for the offset shows that the input-referred offset sigma of the comparator is 14.4 mV. The input-referred offset sigma of the input devices only is found to be 13.9 mV contributing to 97% of the total input-referred offset. This means that contribution of the newly added embedded

regenerative latch is negligible when referred to the input. Keeping this in mind, making the input pair larger will drop down the input-referred offset significantly.

A detailed comparison between the single-ended topology and a conventional StrongARM comparator is shown in Table II. The conventional StrongARM is known to be a low-power structure. For comparison purposes, the input pair dimensions are kept equal between the two designs.

TABLE II. COMPARISON BETWEEN THE PROPOSED COMPARATOR AND STRONGARM COMPARATOR AT 5 GHz.

Comparison Point	StrongARM	This work
Power consumption (μ W)	256	66 (189 for diff-ended)
Max. speed for 5 mV input (GHz)	5	6
Sensitivity at 5 GHz clock (mV)	4	1
3-Sigma Offset(w/o the input pair) (mV)	11.16	0.5

Clock buffers have been designed to drive switches and comparators. The capacitive loading per branch is 160 fF. The power consumption of clock buffers for each interleaved branch is 1 mW. This gives a total power consumption of 4 mW for the clock buffers of the whole ADC. The designed 4-bit 20-GS/s flash ADC has a total power consumption of 15.5 mW. A breakdown of the power consumption of different blocks is given in Table III. Figure 14 shows the frequency response for the ADC output for sinusoidal inputs at 4.84 GHz and 9.84 GHz input frequencies while sampling at an effective frequency of 20 GHz. For the 9.84-GHz input frequency, Table IV summarizes the performance of the whole ADC.

Figure 15 shows the resulting ENOB versus input frequency. It shows a peak ENOB of 3.9 bits at 7.66 GHz input signal.

Small kick-back noise levels allow us to increase the used values of resistors in reference ladder, hence low power consumption for the ladder. DNL and INL for the ADC are shown in Figure 16 and Figure 17 respectively.

Table V shows a detailed comparison between this work and recently published ADCs, it shows that our proposed ADC is the best in class when compared to other high-speed ADCs.

Figure 18 shows the FFT for the output of the whole ADC after parasitic extraction (PEX) working with the highest targeted speed of 20 GS/s. The Flash ADC with its clocking

TABLE III. POWER CONSUMPTION BREAKDOWN.

Ref. ladder	200 μ W
Comparators	11.34 mW
Clock buffers	4 mW
Total Power	15.5 mW

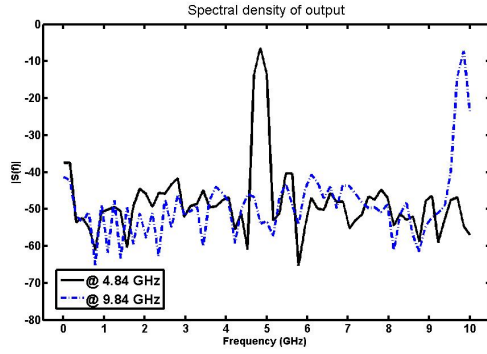


Fig. 14. Frequency Response of Output for Sinusoidal Inputs of 4.84 GHz and 9.84 GHz Input frequencies.

TABLE IV. THE DESIGNED ADC PERFORMANCE SUMMARY.

Sampling frequency	20 GS/s
Input Range	600 mV_{diff}
SFDR	33.58 dB
SNDR	23.86 dB
ENOB (for 9.84 GHz input frequency)	3.67 Bits
Power at Nyquist frequency	15.5 mW
FOMW*	60.8 fJ/conv-step

$$* \text{FOMW} = \frac{\text{Power}}{\text{Sampling rate} * 2\text{ENOB}}$$

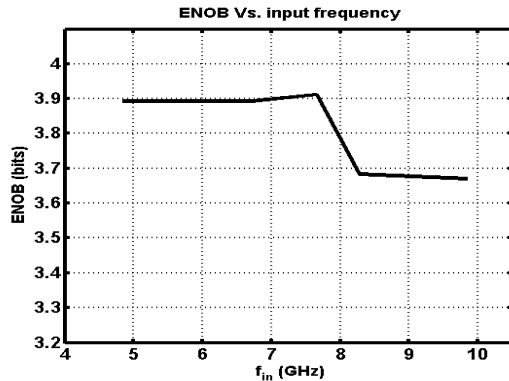


Fig. 15. ENOB Vs. Input Frequency.

system and a testing current steering digital to analog converter (DAC) were laid-out in a total silicon area of $307\mu\text{m} * 124\mu\text{m}$. The layout is as shown in Figure 19.

VII. CONCLUSION

Charge-steering concept is an excellent candidate for high-speed circuits used in analog-mixed signal systems with low power requirements. It proves an advantageous usage over the

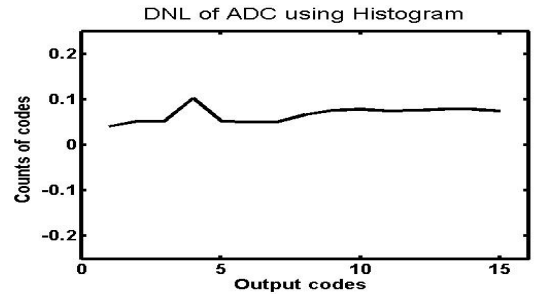


Fig. 16. DNL of the ADC.

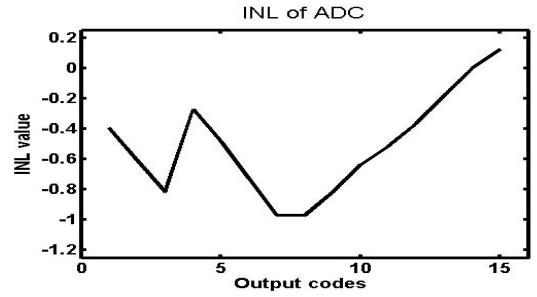


Fig. 17. INL of the ADC.

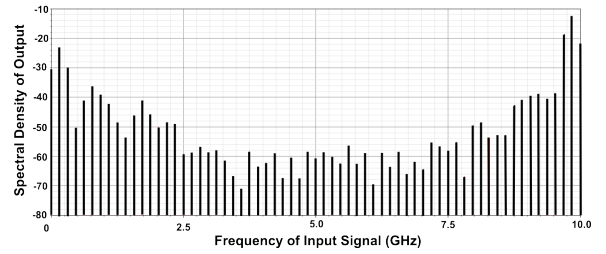


Fig. 18. The Spectral Density of the Extracted-ADC Output.

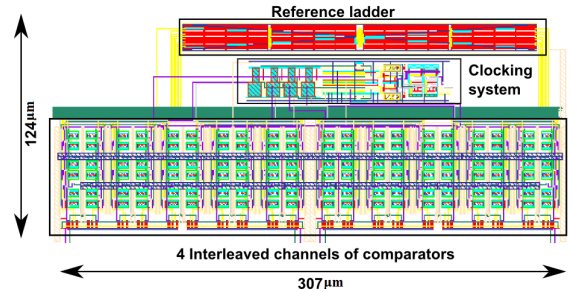


Fig. 19. Layout of the ADC.

current-steering traditional concept, as well as the conventional StrongARM comparator architecture. Charge-steering is used in this paper to design an ultra-low power, $189\text{-}\mu\text{W}$ 5-GHz charge-steering comparator. The proposed idea uses an embedded regenerative latch which is only enabled after the amplification cycle is completed. The input referred offset of this extra latch is negligible compared to the input pair

TABLE V. COMPARISON BETWEEN THIS WORK AND RECENTLY REPORTED FLASH ADCS.

Item	[12]	[13]	[14]	This work
Process	32-nm CMOS	40-nm CMOS	130-nm SiGe	65-nm CMOS
Power (mW)	69.5	500	3000	15.5
Bits	6	N/A	5	4
Sample rate (GS/s)	20	25	22	20
SNDR (dB)	30.7	25.8	20	23.86
FOMW* (fJ/conversion-step)	172.3	1255.8	16695.8	60.8

$$* \text{FOMW} = \frac{\text{Power}}{\text{Sampling rate} * 2^{\text{ENOB}}}$$

offset contribution. Furthermore, the proposed comparator is used to build a 4-bit 4x time-interleaved Flash ADC that works on 20 GS/s sampling rate. ADCs were used to be the bottleneck of the ADC-based receivers. With the ADC designed in this work, ADC's power consumption was as low as 15.5 mW, the thing that paves the way and relieves the burden facing the ADC in the high-speed designs. Moreover, the ADC was preceded by a modified version of a continuous-time linear equalizer, this modified version is called discrete-time linear equalizer (DTLE) and it merges a CTLE with a sample-and-hold network. This equalizer is used after a 12-inch FR4 channel to open the eye diagram of the received signal and enables it to be processed by the ADC and the digital equalizers in a DSP core after that.

REFERENCES

- [1] S. Sheikhaei, S. Mirabbasi, and A. Ivanov, "A 4-bit 5GS/s flash A/D converter in 0.18um CMOS," Proc. IEEE ISCAS, vol. 6, pp. 6138-6141, May 2005.
- [2] A. Ismail, S. Ibrahim and M. Dessouky, "An 8Gbps discrete time linear equalizer in 40nm CMOS technology," IEEE 58th International Midwest Symposium on Circuits and Systems, Fort Collins, CO, pp. 1-4, 2015.
- [3] S. Gondi and B. Razavi, "Equalization and Clock and Data Recovery Techniques for 10-Gb/s CMOS Serial-Link Receivers," IEEE Journal of Solid-State Circuits, vol. 42, no. 9, pp. 1999-2011, 2007.
- [4] B. Razavi, "Charge steering: A low-power design paradigm," Custom Integrated Circuits Conf., pp. 1-8, Sep. 2013.
- [5] Jun Won Jung, Razavi, B., "A 25 Gb/s 5.8 mW CMOS Equalizer," IEEE Journal of Solid-State Circuits, vol.50, no.2, pp. 515,526, Feb. 2015
- [6] Yun-Ti Wang; Razavi, B., "An 8-bit 150-MHz CMOS A/D converter," IEEE Journal of Solid-State Circuits, vol.35, no.3, pp.308,317, March 2000.
- [7] M. M. Ayesh, S. Ibrahim and M. M. Aboudina, "A 15.5-mW 20-GSps 4-bit charge-steering flash ADC," IEEE International Midwest Symposium on Circuits and Systems, Fort Collins, CO, pp. 1-4, 2015.
- [8] S. Babayan-Mashhadi and R. Lotfi, "Analysis and Design of a Low-Voltage Low-Power Double-Tail Comparator," in IEEE Transactions on Very Large Scale Integration (VLSI) Systems, vol. 22, no. 2, pp. 343-352, Feb. 2014.
- [9] B. Razavi, "Design of Analog CMOS Integrated Circuits," NY, USA: McGraw-Hill, 2001.
- [10] T. Toifl et al., "A 2.6 mW/Gbps 12.5 Gbps RX with 8-tap switched-cap DFE in 32 nm CMOS," IEEE Symposium on VLSI Circuits, pp. 210211, 2011.
- [11] Young-Sik Kim et.al., "An 8Gb/s quad-skew-cancelling parallel transceiver in 90nm cmos for high speed dram interface," in IEEE International Solid-State Circuits Conference ISSCC, Feb 2012, pp. 136 138.
- [12] Chen, V.H.-C.; Pileggi, L., "A 69.5mW 20GS/s 6b time-interleaved ADC with embedded time-to-digital calibration in 32nm CMOS SOI," ISSCC Dig. of Tech. Papers, pp.380,381, 9-13 Feb. 2014.
- [13] Crivelli, D., et al. "A 40nm CMOS single-chip 50Gb/s DP-QPSK/BPSK transceiver with electronic dispersion compensation for coherent optical channels," ISSCC Dig. of Tech. Papers, pp.328-330, 6-9 Feb. 2012.
- [14] Schvan, P.; Pollex, D.; Shing-Chi Wang; Falt, C.; Ben-Hamida, N., "A 22GS/s 5b ADC in 130nm SiGe BiCMOS," ISSCC Dig. of Tech. Papers, pp.2340-2349, 6-9 Feb. 2006.